

## Preliminary Design of the Electrical Power Subsystem for the European Student Moon Orbiter Mission

Steve Ulrich, Jean-François Veilleux, and François Landry Corbin  
 Department of Electrical and Computer Engineering, Université de Sherbrooke  
 2500 boul. de l'Université, Sherbrooke (Québec), Canada, J1K 2R1: 819 821-8000, ext. 61215  
 Steve.Ulrich@USherbrooke.ca

### ABSTRACT

The European Student Moon Orbiter (ESMO) spacecraft is a student-built mini satellite being designed for a mission to the Moon. Designing and launching mini satellites are becoming a current trend in the space sector since they provide an economic way to perform innovative scientific experiments and in-flight demonstration of novel space technologies. The generation, storage, control and distribution of the electrical power in a mini satellite represents unique challenges to the power engineer since the mass and volume restrictions are very stringent. Regardless of these problems, every subsystem and payload equipment must be operated within their specified voltage band whenever they require to be turned on. This paper presents the preliminary design of a lightweight, compact, and reliable Electrical Power Subsystem (EPS) for ESMO that can generate 720 W. Some of the key components of the EPS include Ultra Triple-Junction (UTJ) GaAs solar cells controlled by Maximum Power Point Trackers, and high efficiency Li-ion secondary batteries recharged in parallel.

### INTRODUCTION

Since the last few decades, there has been a large interest in operating mini satellites, mainly because they are cheaper to build and to launch. These satellites provide to space agencies and researchers an ideal testbed for in-flight demonstration of innovative and high risk technologies. Used in an educational context, they also prepare students for their future careers in the space sector by giving them valuable hands-on experience. In fact, the number of student-built mini satellites is rapidly growing, especially in Europe and in North America. The MIT's SPHERES<sup>1</sup> (Synchronized Position Hold Engage and Reorient Experimental Satellites) experiment uses the space environment provided by the Space Shuttle and the International Space Station (ISS) in order to validate dynamics and control algorithms for mini satellites in formation. Rendezvous and docking of two SPHERES satellites onboard the ISS has been achieved in 2006.

CanX-1<sup>2</sup> is the first spacecraft developed within the Canadian Advanced Nanospace eXperiment (CanX) program, which was initiated by the University of Toronto in 2001. This technology demonstration spacecraft was a single 'CubeSat' and built according to the California Polytechnic State University (CalPoly) and Stanford University CubeSat standards.<sup>3</sup> Following the successful flight of this 10 x 10 x 10 cm spacecraft, the 3.5 kg milk carton-sized CanX-2<sup>4</sup> will be launched on June 30, 2007 to evaluate technologies that will be used on the expected formation flying mission, CanX-4 / CanX-5.<sup>5</sup>

SSETI Express, which was sponsored by the Student Space Exploration & Technology Initiative (SSETI) association, was successfully launched in October 2005. This first SSETI spacecraft was carrying three CubeSat, a propulsion module, an imaging camera and an amateur radio transponder.<sup>6</sup> Unfortunately, due to an unrecoverable fault in the Electrical Power Subsystem (EPS), the mission was aborted in 2005.<sup>7</sup> The next SSETI satellite is the European Student Earth Orbiter (ESEO), which is planned to be launched in 2008.<sup>8</sup> The European Student Moon Orbiter (ESMO) is the third SSETI spacecraft and was officially approved in 2006 for a phase A study by the Education Department of the European Space Agency (ESA). Just like his SSETI predecessors, ESMO will be completely designed, built, and operated by European and Canadian students in a highly distributed way. This 150 kg satellite will play a valuable role in the international space community, namely by: (1) providing new scientific measurements relevant to lunar science and the future human exploration of the Moon, (2) by providing flight demonstration of innovative space technologies developed under university research activities, and (3) by acquiring images of the Moon for public relations and education outreach purposes. Moreover, it will stimulate space awareness among students and give them technical abilities related to space-oriented projects.

The ESMO spacecraft will be launched either onboard Ariane 5's Arianespace Support for Auxiliary Payload (ASAP) or onboard Soyuz in 2011 from the Guiana

Space Center (GSC) in Kourou. Few thousands of seconds after the launch, ESMO will be separated from the launcher with a spin rate of 5 rpm and deployed in a GTO orbit defined by an inclination ( $i$ ) of  $7^\circ$ , a longitude of ascending node ( $\Omega$ ) of  $10^\circ$  west, an argument of periaapsis ( $\omega$ ) of  $178^\circ$ , an eccentricity ( $e$ ) of 0.716, and a semimajor axis ( $a$ ) of 24630 km. The spacecraft will stay in this GTO phase for one week and then, continuous tangential thrust will start at the last perigee passage. No thrusting will occur during eclipses. This first phase of the mission ends once the apogee reaches 200000 km. From this point, ESMO will use its electric propulsion system and 21 kg of its xenon propellant for delivering 6.5km/s of total  $\Delta V$ , transferring ESMO to its polar lunar orbit in 1 year. The desired stable operational lunar orbit (SOLO) is defined by an inclination ( $i_L$ ) of  $90^\circ$ , an argument of periselenium ( $\omega_L$ ) of  $295^\circ$ , an eccentricity ( $e_L$ ) of 0.481, and a semimajor axis ( $a_L$ ) of 3500 km. Then, the 2 kg primary imager payload will start transmitting data to Earth for a period of approximately 6 months.

Through the last ESA's call for proposals which took place in July 2006, several teams have officially been selected to conduct a phase A study for the ESMO mission. These teams and their responsibility in term of subsystems are defined as follows:

#### **Power**

Université de Sherbrooke, Canada

#### **Payload**

University of Liege, Belgium  
University of Toronto, Canada

#### **Propulsion**

University of Southampton, UK  
University of Warwick, UK  
Politecnico di Milano, Italy  
University di Napoli, Italy

#### **AOCS**

Narvik University College, Norway  
University of Lisbon, Portugal  
SUPAERO, France  
Ryerson University, Canada

#### **On-Board Data Handling**

University of Munich, Germany

#### **Communications**

Wroclaw University of Technology, Poland

#### **Structure**

University of Southampton, UK

#### **Thermal**

Politecnico di Milano, Italy

#### **Mechanisms**

University of Porto, Portugal

#### **Mission Analysis**

University of Glasgow, UK

#### **Ground Segment**

University of Rome, Italy (ground station Kenya)  
University of Munich, Germany (ground station Germany)

#### **Flight Dynamics**

University of Rome, Italy

#### **Simulations**

Warsaw University of Technology, Poland

Contrary to conventional, large satellites that have significant power generation and storage capability, mini satellites such as ESMO do not offer the same advantages, being of small mass. For this reason, most mini satellites are being operated in Earth orbits (LEO or GEO) where large  $\Delta V$ 's and demanding communication power are typically not required. Sometimes, propulsive maneuvers are not even necessary and small thrusters are only used for attitude maneuvers. In that case, the required power may be less than 100 W, which translates a lightweight power system and which is coherent with the philosophy behind the small satellite business. As example, ESA's PROBA-1,<sup>9</sup> a washing machine-size earth observation satellite, operates autonomously with only a few watts.

On the other hand, an interplanetary ESMO-like mini satellite mission that uses ion engines represents a great challenge. Indeed, in order to generate the thrust levels of interest for the mission, the power need is quite high, of the order of 650 - 750 W at beginning of life (BOL). Therefore, given the strict mass constraint imposed by the fact that most mini satellites are launched as piggyback, a state of the art, highly efficient and lightweight EPS becomes mandatory.

This paper presents the preliminary design of the EPS for the ESMO mission conducted by the ESMO's EPS team. The remainder of this paper is as follows. First, salient features of ESMO are given. Thereafter, the mission considerations associated with the EPS design are presented. Next, the functional architecture is outlined and the power budget is detailed. Then, the preliminary design of each element of the EPS; the solar array, the secondary batteries, the power control

unit, and the power distribution unit, are given, respectively. Finally, the conclusion is provided.

### FEATURES OF ESMO

Some of the features of ESMO are:

- Dimensions: 700 mm × 700 mm × 800mm cuboid
- Mass: 150 kg
- Lunar orbit: Polar orbit with a periselenium of 100 km
- Structure: Aluminium alloy honeycomb covered with two skins of CFRP
- Payload: Imaging narrow angle camera (NAC)
- Electric Propulsion: T5 ion engine
- Uplink: 2275 MHz, 2 kbps
- Downlink: 2275 MHz, 2.5 kbps
- Antennas: S-Band omnidirectional × 2
- Transmit power: 5 W
- Attitude control: 3-axis actuation capability
- Thermal: Passive control / radiating panel
- Mission lifetime: 18 months

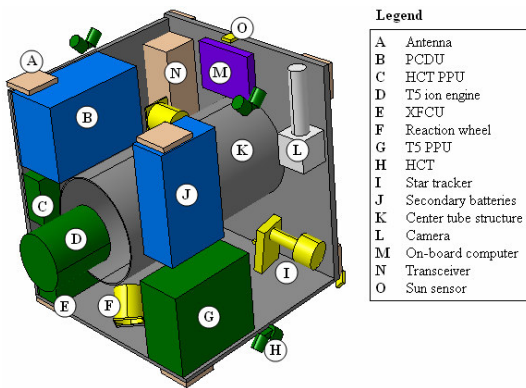


**Figure 1: Internal View of ESMO**

### CONSIDERATIONS FOR THE EPS DESIGN

The EPS for interplanetary mini satellite missions differ from those used in Earth orbits mainly for two reasons: (1) the propulsion system used in the interplanetary phase represents a large power load, and (2) the difference in the mission environment encountered is quite significant. The mission considerations that impact the EPS design for this lunar mission are as follows:

- The Moon is approximately at the same distance from the Sun as the Earth. Therefore, the solar flux in lunar orbit is essentially the same as that in the Earth's orbit.
- The Moon has negligible magnetic field. Therefore, the Sun's charged particles can reach the surface of

the moon without being deflected. The solar array degradation rate will therefore be higher.

- The meteoroid impact rate is also higher in the vicinity of the Moon, yielding a higher rate of mechanical damage on the solar array.
- The nominal SOLO of 5.25 hours is defined by a 5.02 hour period in sunlight and a 0.23 hours period in eclipse.

### FUNCTIONAL ARCHITECTURE

The general layout, or the functional architecture, of the EPS is shown in Figure 2. In this figure, four components of the EPS can be identified: (1) the solar array which generates power, (2) the Power Control Unit (PCU) which conditions the energy, (3) the secondary batteries which are a rechargeable mean of energy storage used for eclipse and peak power demand periods, and (4) the Power Distribution Unit (PDU) which distributes the power to each load, or subsystem, of the spacecraft. All components other than the solar array are located inside the spacecraft body.

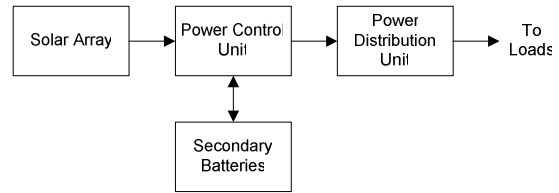


**Figure 2: EPS Functional Architecture**

From the conceptual design presented in a previous work,<sup>10</sup> the EPS team has identified that ESMO will be powered by Ultra Triple-Junction (UTJ) GaAs solar cells controlled by Maximum Power Point Trackers (MPPT). For energy storage, high efficiency Li-ion secondary batteries recharged in parallel will be used. A distributive load regulation approach is also baselined.

### POWER BUDGET

Throughout the mission phases, different subsystems require different power levels in order to operate in a nominal way. Table 1 shows the maximum operating power requirement of every ESMO subsystems. From this table, it is obvious that the main driver for the power generation system sizing is the Power Processing Unit (PPU) of the T5 ion engine. Fortunately, all the subsystems/components do not require to be turned on at the same time during the mission. In order to assess accurately the power consumption throughout the mission, an analysis of dynamic power budgets must be performed. Basically, dynamic power budgets are built,

based on which subsystems are turned on and off for a given period of time. Dynamic power budgets were built for the three critical mission phases, which were defined from an EPS perspective: (1) initial operations in Low Earth Orbit Phase (LEOP), (2) injection into SOLO, and (3) SOLO phase.

In early LEOP, several check-up and routine operations must be performed, such as de-spin, sun acquisition, and solar array deployment. Because all these early operations are achieved with unfolded solar panels, no energy coming from the Sun can be converted into electricity. ESMO will then have to rely entirely on its energy storage system.

The injection into SOLO is a critical phase since thrusting maneuvers are required to place ESMO into the desired final lunar orbit. Orbital elements of this phase are considered to be the same as those of the SOLO phase. During the injection into SOLO, the T5 ion engine is expected to operate in its low power mode during attitude maneuvers (where the Hollow Cathode Thruster are used) and during eclipse periods. The maximum power demand during this phase is of 663 W.

Finally, the SOLO phase is quite similar to the SOLO injection phase, except that during SOLO, the T5 ion engine is turned off. Also, the imaging camera is assumed to be used for 30 minutes around the periselenium followed by a 1 hour TX activity around the aposelenium to send back to Earth the stored data.

The details of the power requirement for each of these three mission phases are given in Table 2 to 4 and illustrated in Figure 3 to 5. It should be noted that in these figures, some parts of the graphs have been highlighted in gray to illustrate the eclipse periods. After a closer analysis of these tables and figures, it can be concluded the LEOP and the SOLO injection phase represent the sizing case for the battery and for the solar array, respectively. Considering power losses, array degradation, and the battery charge power with some margins, the required solar array output is estimated to 720 W at BOL. The computation of the required battery capacity will be performed later.

### SOLAR ARRAY

The design of the solar array presents unique challenges to the power system engineer since the mass and volume available are all very limited. However, in the last years, solar cells manufacturers have greatly improved cell efficiency and power production. Solar cells with greater than 28% efficiency are now commercially available. With multi-junction cells, layers of different materials and doping levels are used

**Table 1: Operating Power Requirement Values**

Subsystem/Component	Power (W)
<b>AOCS</b>	
Star Tracker	4.0
Gyroscope	1.0
Reaction Wheels	12.0
<b>Communications</b>	
Receiver (Rx) and RF Distribution Unit	6.0
Transmitter (Tx)	25.0
<b>On-Board Data Handling</b>	
On-Board Computer	22.0
<b>Payload</b>	
Narrow Angle Camera	10.0
<b>Propulsion</b>	
T5 Ion Engine PPU – HIGH	600.0
T5 Ion Engine PPU – LOW	38.0
Hollow Cathode Thruster (HCT) PPU	80.0
<b>Power</b>	
Power Control Unit (PCU)	7.0
Power Distribution Unit (PDU)	3.0
Battery Heaters	60.0
<b>Mechanism</b>	
Solar Array Drive Mechanism (SADM)	9.0

to extract energy from different portions of the light spectrum, converting more of the spectrum into power.

For the ESMO spacecraft, the proposed solar array consists of UTJ GaAs solar cells manufactured by Boeing Spectrolab, which have an efficiency of 28.3% at BOL and of 24.3% at EOL.<sup>11</sup> The UTJ GaAs cell consists of Ge, GaAs, and GaInP<sub>2</sub> semiconductors interconnected by two tunnel junctions, as illustrated in Figure 3.

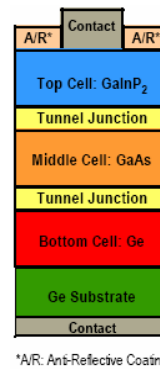


**Figure 3: UTJ GaAs Cell<sup>11</sup>**

**Table 2: Power Requirement for Initial LEOP Operation Phase**

Subphase	Power (W)	Duration (hrs)
Separation and AOS	28.0	5.00
Check-Up	53.0	1.00
De-Spin	54.0	0.50
Sun Acquisition	47.0	0.50
Solar Array Deployment	63.0	0.25

**Table 3: Power Requirement for SOLO Orbital Injection Phase**

Component	Subphase				
	A	B	C	D	E
Star Tracker					
Gyroscope					
Reaction Wheels					
Receiver (Rx) and RF Dist. Unit					
Transmitter (Tx)					
On-Board Computer					
Narrow Angle Camera					
T5 Ion Engine PPU - HIGH					
T5 Ion Engine PPU - LOW					
Hollow Cathode Thruster PPU					
Power Control Unit					
Power Distribution Unit					
Heaters					
Solar Array Drive Mechanism					

**Table 4: Power Requirement for SOLO Phase**

Component	Subphase						
	A	B	C	D	E	F	G
Star Tracker							
Gyroscope							
Reaction Wheels							
Receiver (Rx) and RF Dist. Unit							
Transmitter (Tx)							
On-Board Computer							
Narrow Angle Camera							
Ion Engine PPU - HIGH							
Ion Engine PPU - LOW							
Hollow Cathode Thruster PPU							
Power Control Unit							
Power Distribution Unit							
Heaters							
Solar Array Drive Mechanism							

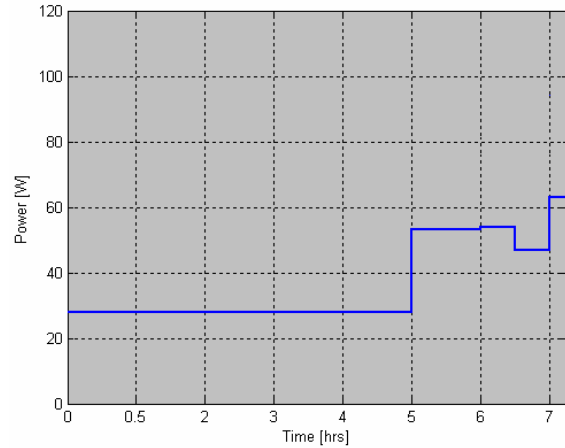


**Figure 4: Power Requirement for Initial LEOP Operation Phase**

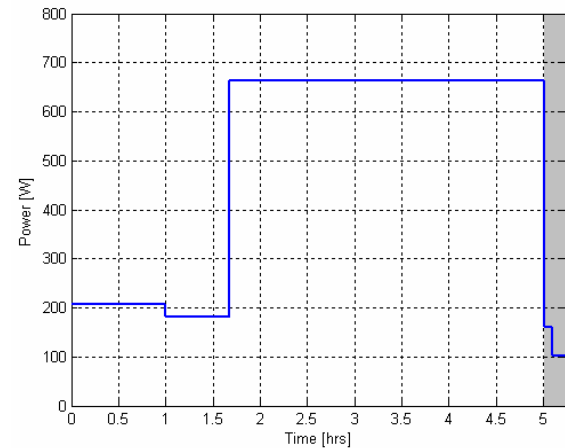


**Figure 5: Power Requirement for SOLO Orbital Injection Phase**

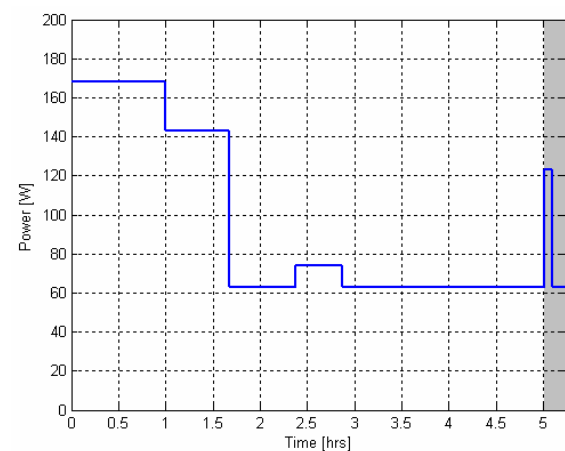


**Figure 6: Power Requirement for SOLO Phase**

### I-V Characteristics

The performance of a solar cell at BOL is mainly characterized by the output voltage and current at its terminals, which can be determined by an accurately measured I-V characteristics curve of the solar cell. Figure 7 illustrates the I-V curve for an UTJ cell, as supplied by Spectrolab<sup>11</sup>.

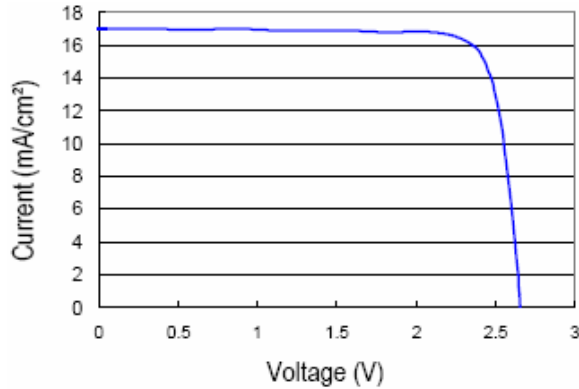


**Figure 7: I-V Characteristics of an UTJ GaAs cell<sup>11</sup>**

On this curve, the two extreme points, the open circuit voltage  $V_{OC}$  and the short circuit current  $I_{SC}$  are of a great importance. Indeed, the maximum power  $P_{max}$  that can be generated by the cell is given by the following equation:

$$P_{max} = CFF \times V_{OC} \times I_{SC} \quad (1)$$

where the curve fill factor (CFF) defines the quality of the voltage-current characteristics. From Figure 7,  $V_{OC}$  is 2.665 V,  $I_{SC}$  is 17.05 mA/cm<sup>2</sup> and the maximum power point (MPP) is located at 2.350 V ( $V_{MP}$ ) and at 16.30 mA/cm<sup>2</sup> ( $I_{MP}$ ). From Spectrolab's data sheet,<sup>11</sup> the CFF is 0.84. Therefore, from Eq. (1),  $P_{max}$  is 0.03816 W/cm<sup>2</sup>.

### Array Design

The solar cells on the array are segmented in many strings connected in parallel. The following equations can be used to determine the parameters needed to design the array:

$$N_{series\ cells\ per\ string} = \frac{array\ voltage}{V_{mp}} \quad (2)$$

$$N_{parallel\ panels} = \frac{array\ current}{I_{panel}} \quad (3)$$

$$N_{strings\ per\ panel} = \frac{I_{panel}}{I_{mp}} \quad (4)$$

With a desired array voltage equal to 28 V and using the numerical value of  $V_{MP}$  defined in the previous subsection, Eq. (2) yields a total of 12 cells in series per string. Considering that six panels (three per wing) will be used on ESMO, and that the array current must be equal to 25.7 A in order to generate the required 720 W, Eq. (3) gives a panel current ( $I_{panel}$ ) of 4.3 A. Finally, assuming a cell size of 24 cm<sup>2</sup> (5.5 cm × 4.4 cm), Eq. (4) gives 11 strings per panel. The resulting configuration of the cells on a single panel is illustrated in Figure 8.

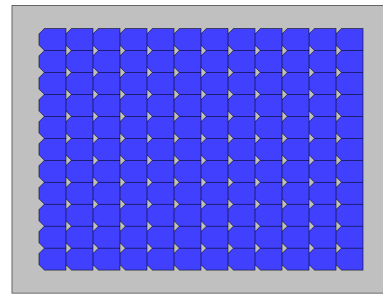


**Figure 8: 765 mm × 567 mm Rigid Solar Panel**

The total size of one rigid panel is 765 mm × 567 mm (including some margins around the cells), which respects the maximum allowed size of 800 mm × 600 mm. Since the effective area of a single panel is 3146 cm<sup>2</sup>, each panel will generate ~120 W for a total of 720 W for six panels. Both sets of three rigid panels will be initially stowed with the spacecraft during the launch and will be deployed using the Solar Array Deployment Mechanism (SADM) described in Calassa's work.<sup>12</sup> The Calassa's SADM has the advantage of being lightweight while being produced and installed at the lowest possible cost.

### SECONDARY BATTERIES

Lithium-Ion (Li-ion) battery cells were chosen for ESMO mainly because they provide the best compact and weight-saving solution to ensure continuous operation of spacecraft at times when the solar cells are not in sunlight or when peak-power demands exceed the power generated by the solar array (namely before the solar array deployment).<sup>10</sup> In comparison to other type of secondary batteries, Li-ion batteries have the following advantages:

- Their high density of energy (twice as much as NiH<sub>2</sub>) provides a significant saving of weight

(approximately 30% to 50%). This reduction in weight leaves more room for larger payloads.

- Li-ion batteries do not require reconditioning since they do not suffer from memory effect.
- Li-ion's low thermal radiation enables the use of smaller battery radiators, which further reduces the EPS weight.
- Li-ion batteries retain their charge for longer period, thus do not require charging while awaiting the launch. This reduction in launch pad operations contributes to the overall mission cost reduction.

As explained by Patel,<sup>13</sup> the electrical performance requirement of the secondary batteries depends on the electrochemistry and on many other parameters in a highly nonlinear manner. In fact, this is why the battery design is one of the most difficult tasks for the power system engineer. However, the required capacity of the secondary battery, in Whr, can be estimated with a simple relation, as follows:

$$Cr = \frac{1}{nDOD} \sum_{i=1}^5 P_i T_i \quad (5)$$

where the  $\sum_{i=1}^5 P_i T_i$  term represents the ideal capacity;

the summation of power load (in W) times the duration (in hrs) for each of the five initial LEOP operation subphases (check-up, de-spin, etc.). This ideal capacity is then increased to include the battery-to-load transmission efficiency,  $n$ , and the depth-of-discharge constraint, DOD. The DOD is defined as the percentage of the battery capacity discharged during an eclipse period. The required DOD is typically based on the type of mission. In the case of a rapid cycling LEO satellite, the DOD will be limited in order to not overstress the batteries. For a GEO satellite, it will be higher as the



Figure 9: SAFT MPS 176065 Cell<sup>14</sup>

battery is only used a few days per year. Considering the nature of this specific mission, where a few thousand of cycles will occur, the maximum DOD has been fixed to 50%. The transmission efficiency is considered to be 90%.

Using Eq. (5) with the numerical values given in Table 2, the ideal capacity requirement during the initial LEOP operation phase is 265 Whr. With the DOD and efficiency considerations, the required battery capacity is 589 Whr, or 21 Ahr at 28 V.

Table 5: SAFT MPS 176065 Cell Characteristics

Cell Characteristic	Value
Capacity, Ahr	5.80
Capacity, Whr	20.00
Voltage, V	3.80
Specific Energy, W/kg	133.00
Weight, kg	0.15
Height, mm	65.00
Depth, mm	15.00
Width, mm	65.00

The baseline battery uses SAFT MPS 176065 Li-ion cells<sup>14</sup>. The specifications of these cells are given in Table 5. In order to generate the required bus voltage of 28 V, eight 3.8 V cells in series must be used and four cells in parallel are necessary to get the required capacity of 21 Ahr. Considering that there should be an additional string of cells to overcome possible short-circuits and loss of a complete string, an additional string of cells in parallel is added, yielding an 8s5p configuration. Including some margin, the battery weight will be around 2.2 kg.

## POWER CONTROL UNIT

In order to fully optimize the power/mass ratio of the mini satellite, a commercial off-the-shelf (COTS) Power Control Unit (PCU) is not considered suitable for the ESMO mini satellite. Instead, a custom-built PCU tailored to the mission's constraints is considered as the baseline solution.

The PCU consists of the following components: two Maximum Power Point Tracker Units (MPPTU), a Battery Monitor (BM), and a Power Management Unit (PMU). The internal and external interfaces between the components of the PCU are illustrated in Figure 10.

The two MPPTs are used to interface the power from the two solar arrays to the main ~28V unregulated power bus and the Li-ion batteries will be interfaced directly to the main power bus through the BM, which

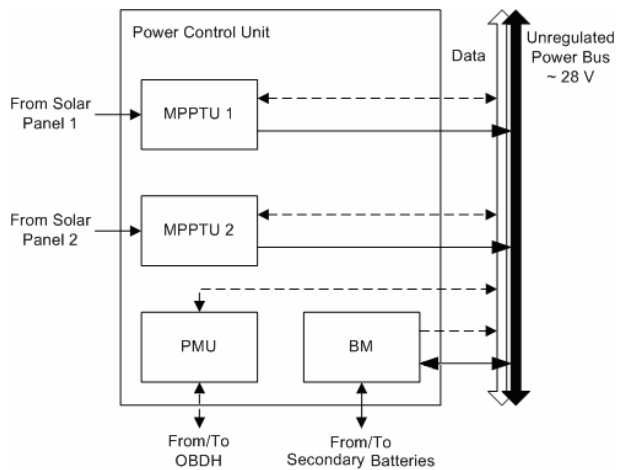


**Figure 10: Internal and External Interfaces of the PCU**

monitors the state-of-charge and to prevent the overcharging of the batteries. The PMU basically fulfills the functions of a telecommand and telemetry module (TC/TM). In this section, the design of these three PCU components is presented.

#### Maximum Power Point Tracker Unit

The MPPTU functionality is to monitor the voltage and current output of the solar array at all times, in order to force the solar array output to operate at the Maximum Power Point (MPP). To do so, a DC-DC converter in a given configuration is first used. Then, with an MPPT algorithm implemented in a dedicated microprocessor, the peak power operating point of the solar array on its I-V curve is detected and tracked.

#### DC-DC Converter

Typical DC-DC converter configurations are the Boost, the Buck, and the Boost-Buck and a series of hybrid versions of those. An overview of all of those configurations can be found in Walker's work.<sup>15</sup>

As with any other EPS components, redundancy should be limited to the minimum, in order to reduce the mass as much as possible. Therefore, typical serial configurations are considered too risky. Indeed, a failure of a series-connected DC-DC converter would prevent the current to flow, creating a disconnection between the solar arrays and the main power bus, causing a major failure of the EPS.

The series connected boost converter (SCBC), which simple principle of operation is explained elsewhere,<sup>16</sup> overcome this problem. As illustrated in Figure 11, if a converter failure occurs, the current would still flow

from the solar arrays to the power bus. The solar array voltage would just not be conditioned anymore. That situation can quickly become a serious problem if the solar arrays and the secondary battery are operated at different voltage levels. However, for ESMO, because the operating voltage of the solar arrays has been fixed to match the battery voltage, a converter failure would only cause an uncontrolled charging of the battery, thus slightly reducing their operational lifetime.

Another great advantage of this configuration is its great efficiency; around 95 - 98% in comparison to 85 - 90% available with the standard converter topologies.<sup>15</sup> This translates directly into mass and costs saving. Finally, the SCBC configuration is considered the baseline solution to provide a simple and reliable way to achieve a high efficiency and a fault tolerant DC-DC conversion for ESMO.

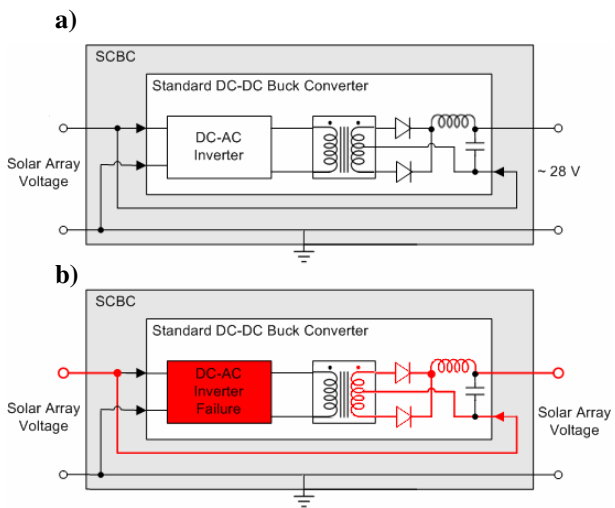


**Figure 11: a) Schematic of a Functional SCBC  
b) Functionality in a Case of a Failure**

#### MPPT Algorithm

Nowadays, several MPPT algorithms are available and can be considered by the power engineer. However, many of them are still under development. Every single algorithm has its own advantages and drawbacks has discussed in Chapman's survey on MPPT algorithms.<sup>17</sup> In order to ensure robust and risk-free MPPT operations, only well known and in-flight demonstrated MPPT algorithms are considered for this mission to the Moon. These are the so-called Perturb and Observe (P&O) algorithm and the Incremental Conductance (IncCond) algorithm.

The fundamental principle of operation of a P&O MPPT algorithm is to generate a perturbation in the operating voltage of the solar array, and to observe the

resulting gain (or loss) on the output power. This technique is very similar to the hill-climbing method<sup>18, 19</sup> which generates a perturbation in the duty cycle, thus producing a perturbation in the operating voltage of the solar array. The P&O algorithm is one of the easiest algorithms to implement, in which both current and voltage are monitored for computation needs. The speed of convergence toward the MPP varies according to the perturbation frequency. Smaller step between perturbations offer a faster tracking algorithm, but yields oscillations around the MPP once reached, causing loss of power. For better performance, the P&O algorithm can be implemented in a two-stage algorithm including a fast tracking stage and then a slow, finer tracking stage, to keep a good convergence speed and to limit the power loss of fluctuation around the MPP.<sup>17</sup>

The second algorithm, the incremental conductance (IncCond) algorithm, is based on the fact that the slopes of the power-voltage array power curve is zero at the MPP, positive on the left of the MPP, and negative on the right, as given by:

$$\begin{cases} dP / dV = 0, & \text{at MPP} \\ dP / dV > 0, & \text{left of MPP} \\ dP / dV < 0, & \text{right of MPP} \end{cases} \quad (6)$$

Since

$$dP / dV = I + VdI / dV \cong I + V\Delta I / \Delta V \quad (7)$$

Eq. (6) can be rewritten as:

$$\begin{cases} \Delta I / \Delta V = -I / V, & \text{at MPP} \\ \Delta I / \Delta V > -I / V, & \text{left of MPP} \\ \Delta I / \Delta V < -I / V, & \text{right of MPP} \end{cases} \quad (8)$$

Hence, the MPP can be tracked by comparing the instantaneous conductance ( $I/V$ ) to the incremental conductance ( $\Delta I/\Delta V$ ).

As with the P&O algorithm, the increment size determines the convergence of the IncCond algorithm speed toward the MPP and the oscillation around it. A two-stage solution can also be implemented to overcome oscillation problems. Moreover, this two-stage solution ensures that the real MPP is tracked in case of multiple local maxima. Again, this technique must monitor current and voltage, but since this slightly more complex method gives a better accuracy and efficiency compared to the P&O, this technique has been selected for the ESMO spacecraft's PCU.

### Battery Monitor

Since the secondary battery is a critical component in ESMO's EPS, monitoring its state of health is important. This is done with the Battery Monitor (BM). Because the choice of using a MPPT led to the choice of an unregulated power bus,<sup>10</sup> the battery is directly connected to it through the Battery Monitor (BM). Although complex techniques such as neural network and fuzzy logic can be used for this purpose,<sup>20</sup> the typical approach consists of using a voltage and a current sensor. This typical BM monitors the battery's voltage and current drawn (which is also used as the power bus monitor since it is directly connected to it). This type of BM enables the control of the state-of-charges of the batteries by the MPPT and prevents battery overcharging (by adjusting the point of operation needed for both solar arrays).

For efficiency reasons, the current sensor will be a commercial off-the-shelf (COTS) Hall Effect Current Sensor (HECS). It can either be an open-loop or closed-loop sensors. Open-Loop sensors can be a good choice, but Close-Loop current sensors offer higher accuracy by correcting the linearity and gain errors through a negative feedback. Since both versions cost about the same price for a nominal current specification, the decision of using closed-loop HECS for ESMO was made. Moreover, this type of sensor represents a simple and efficient way to monitor the current source to or sink from the battery.



**Figure 12: Tamura S22P025S05 Hall Effect Current Sensor<sup>21</sup>**

Tamura Corp. produces a great variety of COTS HECS which are commonly available, thus reducing their price. The S22P025S05,<sup>21</sup> which is illustrated in Figure 12, represents an attractive and affordable baseline solution.

### Power Management Unit

The Power Management Unit (PMU) on-board ESMO will be used as a telecommand and telemetry module (TC/TM) to: (1) decode commands from OBDH in

order to switch loads on and off, and (2) to send monitoring data back to OBDH. Considering the inherent complexity of this component, a COTS solution is adopted. Moreover, this solution will reduce the risk of a PMU failure which would be critical for the mission.

The different COTS TM/TC modules currently considered are the following: the Alcatel Space TMTC-H5 and TMTC-S3 (both from the 9353 modular PCDU)<sup>22</sup> and the TERMA Command and Monitoring (CM) module.<sup>23</sup>

The Alcatel Space TMTC-S3 offers a low-mass (1.25kg) and compact design (340x190x25.5mm) with all the required features for the ESMO mission. Moreover, between the three considered options, it's the only one that offers a RS422 bus interface as required by the ESMO OBDH. For all these reasons, for its ease of implementation and for its good reliability, the TMTC-S3 PMU is selected for ESMO.

### POWER DISTRIBUTION UNIT

The Power Distribution Unit (PDU) provides switch control and protection between the main bus and the loads connected to it. Considering that the main power bus is unregulated at ~28V and that most subsystems already have their own regulator, a distributive regulation approach is adopted.

For over-current protection, current limiters or fuse-relays can be used. Because of their higher flexibility, ease of testing and rearming capabilities over fuse-relays, current limiters are baselined for ESMO. A trade-off analysis between these two protection devices can be found elsewhere.<sup>24</sup> Two type of current-limiter are necessary: fold-back current limiters (FCL) for vital subsystems (EPS, OBDH, COMM, etc.) and latching current limiters (LCL) for the other loads (propulsion, hollow cathode thruster PPU, reaction wheels, payloads, etc.). Some FCL can also be designed using the LCL configuration with automatic re-trigger circuit.

However, these devices can be quite complex to design (electronically and thermally speaking). But, by using a COTS PDU, such as the Alcatel Space LCL and Heaters distribution module (H3 or P2)<sup>22</sup> the TERMA Power Distribution Module (PDM),<sup>23</sup> the design complexity drawback can be avoided. The Alcatel Space P2 module offers 9 LCL up to 10A each, one permanent-on LCL up to 5A, 1 FCL up to 1A and 2 heater group switch up to 10A (which are all found to be well-suited for ESMO which requires 10 LCL/FCL as well as heaters). This module also offers a low-mass (1.25kg) and compact design (340x190x25.5mm) with all the main performances required. Moreover, this

solution offers the advantage of being easily implemented with the TMTC-S3 PMU since they are both from the same manufacturer and are meant to be used together in a modular PCDU.

### CONCLUSION

In this paper, the preliminary design of a lightweight, compact, and reliable EPS for the ESMO mini satellite has been presented. Thanks to key components such as the Ultra Triple-Junction (UTJ) GaAs solar cells and the Li-ion secondary battery, ESMO's EPS will be able to provide the required energy to all subsystems, even during thrusting and eclipse periods. Whenever possible, the EPS design for this mission to the Moon has been performed by selecting flight-proven solutions and technologies, increasing as much as possible the reliability of the EPS, and thus of the entire spacecraft and mission.

### ACKNOWLEDGEMENTS

The authors wish to thank each member of the ESMO mission for their contributions and dedication to the development of the ESMO spacecraft, and to Roger Walker from ESA for his invaluable mentorship.

### REFERENCES

1. "SPHERES as a Formation Flight Algorithm Development and Validation Testbed: Current Progress and Beyond," Proceedings of the 2nd International Symposium on Formation Flying Missions & Technologies, Washington, DC, 14-16 September, 2004.
2. Stras L. N., Kekez D. D., Wells G. J., Jeans T., Zee R. E., Pranajaya F. M., and Foisy D. G., "The Design and Operation of The Canadian Advanced Nanospace eXperiment (CanX-1)," Proceedings of AMSAT-NA 21st Space Symposium, Toronto, Canada, October, 2003.
3. Twiggs R. J., Shinichi N. et al., "A CubeSat: A New Generation of Picosatellite for Education and Industry Low-Cost Space Experimentation," Proceedings of the 14th AIAA/USU Conference on Small Satellites, Logan, Utah, August, 2000.
4. Sarda K., Eagleson S., Caillibot E. P., Grant C., Kekez D. D., Pranajaya F., and Zee R. E., "Canadian Advanced Nanospace Experiment 2: Scientific and Technological Innovation on a Three-Kilogram Satellite," Acta Astronautica, Vol. 59, 2006, pp. 236-245.
5. Sarda K., Eagleson S., Mauthe S., Tuli T., Zee R. E., Grant C. C., Foisy D. G., Cannon E., and Damaren C. J., "CanX-4 & CanX-5: Precision Formation Flight Demonstrated by Low Cost

- Nanosatellites,” Proceedings of the 13th Canadian Astronautics Conference, Montreal, Canada, April, 2006.
6. Alminde L., Bisgaard M., Melville N., and Schaefer J., “The SSETI-express Mission: From Idea to Launch in one and a Half Year,” Proceedings of the 2nd International Conference on Recent Advances in Space Technologies,” Istanbul, Turkey, 9-11 June, 2005.
  7. “SSETI Express: Power Problem,” [http://www.esa.int/SPECIALS/sseti\\_express/SEM9NC638FE\\_0.html](http://www.esa.int/SPECIALS/sseti_express/SEM9NC638FE_0.html), ESA, 31 October, 2005.
  8. Viscor T., “SSETI - Past, Present and Future,” Proceedings of the 20th AIAA/USU Conference on Small Satellites, Logan, Utah, 14-17 August, 2006.
  9. Teston F., Creasy R., Bermyn J., Mellab K., “PROBA: ESA’s Autonomy and Technology Demonstration Mission,” Proceedings of the 48th International Astronautical Congress, Turin, Italy, 6-10 October, 1997.
  10. Ulrich S., Corbin F. L., and Côté H. N., “Conceptual Design of the Electrical Power Subsystem for the European Student Moon Orbiter Mission,” Proceedings of the 57th International Astronautical Congress, Valencia, Spain, 2-6 October, 2006.
  11. “28.3% Ultra Triple Junction (UTJ) Solar Cells,” <http://www.spectrolab.com/DataSheets/TNJCell/utj3.pdf>, Spectrolab, 2004.
  12. Calassa M. C, and Kackley R., “Solar Array Deployment Mechanism,” Proceedings of the 29th Aerospace Mechanisms Symposium, 1995.
  13. Patel M. R., “Spacecraft Power Systems,” CRC Press, 2005.
  14. “Rechargeable Li-ion battery systems,” [www.saftbatteries.com/I30-Catalogue/PDF/space li-ion.pdf](http://www.saftbatteries.com/I30-Catalogue/PDF/space_li-ion.pdf), SAFT, October 2006.
  15. Walker G. R., and Sernia P. C., “Cascaded DC-DC Converter Connection of Photovoltaic Modules,” IEEE Transactions on Power Electronics, Vol. 19, No. 4, July 2004.
  16. Nadkarni A. A., Beltran E., and Pillar S. L., “Preliminary Design Review Report for the DAWGSTAR Project,” University of Washington, 8 June, 1999.
  17. Chapman P. L., and ESRAM T., “Comparison of Photovoltaic Array Maximum Power Point Tracking Techniques,” IEEE Transactions on Energy Conversion, Vol. 22, Issue 2, June 2007.
  18. Teulings W. J. A., Marpinard J. C., Cape A. I, and O’Sullivan D., “A new maximum power point tracking system,” Proceedings of the 24th Annual IEEE Power Electronic Specialists Conference, 1993.
  19. Xiao W., and Dunford W. G., “A modified adaptive hill climbing MPPT method for photovoltaic power systems,” Proceedings of the 35th Annual IEEE Power Electronic Specialists Conference, 2004.
  20. Kozłowski J. D., Watson M. J., Byington C. S., Garga A. K., and Hay T. A., “Electrochemical Cell Diagnostics Using On-Line Impedance Measurements, State Estimation and Data Fusion Techniques,” Proceedings of the 36th Intersociety Energy Conversion Engineering Conference, ASME, 2001.
  21. “Hall Effect Current Sensors,” <http://www.tamuracorp.com/clientuploads/pdfs/pgs85-86.pdf>, TAMURA Corp, 2005.
  22. “Alcatel 9353 Power Conditioning and Distribution Unit, Medium Power,” [http://www1.alcatel-lucent.com/space/etca/activities/\\_sob/pdf/s\\_2.pdf](http://www1.alcatel-lucent.com/space/etca/activities/_sob/pdf/s_2.pdf), Alcatel Alenia Space, January 2006.
  23. “Command and Monitoring Module,” [http://www.terma.com/multimedia/CM\\_Flyer1.pdf](http://www.terma.com/multimedia/CM_Flyer1.pdf) TERMA Space, September 2004.
  24. Rubel W., “Satellite Design, Power System,” <http://www.irs.uni-stuttgart.de/skript/KSE/KSE-WS061117.pdf>, EADS Astrium, November 2006.